THE JOURNAL OF BIOLOGICAL CHEMISTRY VOL. 281, NO. 39, pp. 29256–29267, September 29, 2006

Substrate and Product Trafficking through the Active Center Gorge of Acetylcholinesterase Analyzed by Crystallography and Equilibrium Binding*

Received for publication, March 30, 2006, and in revised form, July 5, 2006 Published, JBC Papers in Press, July 12, 2006, DOI 10.1074/jbc.M603018200

Yves Bourne[‡1], **Zoran Radić**[§], **Gerlind Sulzenbacher**[‡], **Esther Kim**[§], **Palmer Taylor**[§], **and Pascale Marchot**[¶2]

From the [¶]*Ingénierie des Protéines, CNRS FRE-2738, Institut Fédératif de Recherche Jean Roche, Université de la Méditerranée, Faculté de Médecine Secteur Nord, F-13916 Marseille Cedex 20, France, the* [‡]*Architecture et Fonction des Macromolécules Biologiques, CNRS UMR-6098, Campus Luminy, Case 932, F-13288 Marseille Cedex 09, France, and the* [§]*Department of Pharmacology, University of California at San Diego, La Jolla, California 92093-0636*

Hydrolysis of acetylcholine catalyzed by acetylcholinesterase (AChE), one of the most efficient enzymes in nature, occurs at the base of a deep and narrow active center gorge. At the entrance of the gorge, the peripheral anionic site provides a binding locus for allosteric ligands, including substrates. To date, no structural information on substrate entry to the active center from the peripheral site of AChE or its subsequent egress has been reported. Complementary crystal structures of mouse AChE and an inactive mouse AChE mutant with a substituted catalytic serine (S203A), in various complexes with four substrates (acetylcholine, acetylthiocholine, succinyldicholine, and butyrylthiocholine), two non-hydrolyzable substrate analogues (*m*-(*N,N,N*-trimethylammonio)-trifluoroacetophenone and 4-ketoamyltrimethylammonium), and one reaction product (choline) were solved in the 2.05–2.65-Å resolution range. These structures, supported by binding and inhibition data obtained on the same complexes, reveal the successive positions and orientations of the substrates bound to the peripheral site and proceeding within the gorge toward the active site, the conformations of the presumed transition state for acylation and the acyl-enzyme intermediate, and the positions and orientations of the dissociating and egressing products. Moreover, the structures of the AChE mutant in complexes with acetylthiocholine and succinyldicholine reveal additional substrate binding sites on the enzyme surface, distal to the gorge entry. Hence, we provide a comprehensive set of structural snapshots of the steps leading to the intermediates of catalysis and the potential regulation by substrate binding to various allosteric sites at the enzyme surface.

The principal role of acetylcholinesterase (AChE)[3] at cholinergic synapses is to terminate neurotransmission by fast hydrolysis of the substrate, acetylcholine (ACh) (1, 2). The AChE active center, containing the catalytic triad, Glu^{334}-His^{447}-Ser^{203} in mammals (3), is located centrosymmetric to the subunit and at the base of a deep and narrow gorge (4, 5).

AChE-catalyzed hydrolysis of ACh and other carboxyl esters proceeds via formation of an initial noncovalent enzyme-substrate complex. Nucleophilic attack of the substrate carbonyl carbon by the Ser^{203} hydroxyl generates a transient tetrahedral oxyanion intermediate, which collapses into a short-lived ($t_{½} \sim 50\ \mu s$) acyl-enzyme (ester) intermediate and a released choline molecule (6). Deacylation through hydrolytic attack on the ester carbonyl by a water molecule leads to a second tetrahedral intermediate, which then collapses into a regenerated enzyme and an acetate molecule. Rapid rates of substrate association and choline product dissociation contribute to the AChE high specific activity and catalytic throughput. Ser^{203} is rendered more nucleophilic by catalytic triad residues Glu^{334} and His^{447}. Residue Trp^{86}, located at the very base of the active center gorge, orients the ACh trimethylammonium group prior to hydrolysis, whereas the oxyanion hole amide hydrogens from Gly^{121}, Gly^{122}, and Ala^{204}, presumably stabilize the carbonyl oxygen of ACh in the transition states for acylation and deacylation.

Inhibitors of AChE bind to the active site or to the peripheral anionic site (PAS), an allosteric site located at the active center gorge entrance, or they span the two sites thereby occupying much of the active center gorge (7–9). PAS inhibitors limit the catalytic rate by steric and electrostatic blockade of ligand trafficking through the gorge and by altering the active center conformation (10–14). Mutagenesis and structural studies have revealed the functional role of residues Tyr^{72}, Asp^{74}, Tyr^{124}, Trp^{286}, and Tyr^{341} at the PAS (5, 15–20).

Kinetics of cationic substrate hydrolysis catalyzed by AChE deviate from Michaelis-Menten kinetics (21, 22). Cationic sub-

* This work was supported by United States Public Health Service Grant R37-GM18360 and Department of Army Medical Defense Grant 17-1-8014 (to P. T.) and the Association Française contre les Myopathies (to P. M.). The costs of publication of this article were defrayed in part by the payment of page charges. This article must therefore be hereby marked "*advertisement*" in accordance with 18 U.S.C. Section 1734 solely to indicate this fact.

The atomic coordinates and structure factors (codes 2H9Y, 2HA0, 2HA2, 2HA3, 2HA4, 2HA5, 2HA6, and 2HA7) have been deposited in the Protein Data Bank, Research Collaboratory for Structural Bioinformatics, Rutgers University, New Brunswick, NJ (http://www.rcsb.org/).

[1] To whom correspondence may be addressed. Tel.: 33-491-825-566; Fax: 33-491-266-720; E-mail: Yves.Bourne@afmb.univ-mrs.fr.

[2] To whom correspondence may be addressed. Tel.: 33-491-698-908; Fax: 33-491-657-595; E-mail: marchot.p@jean-roche.univ-mrs.fr.

[3] The abbreviations used are: AChE, acetylcholinesterase; (mAChE, recombinant from mouse; S203A, mutant from mouse; TcAChE, from *T. californica*); BChE, butyrylcholinesterase; ACh, acetylcholine; ATCh, acetylthiocholine; BTCh, butyrylthiocholine; SCh, succinyldicholine; 4K-TMA, 4-ketoamyltrimethylammonium; PAS, peripheral anionic site; r.m.s., root mean square; TCh, thiocholine; TMTFA, *m*-(*N,N,N*-trimethylammonio)trifluoroacetophenone; Mes, 2-(*N*-morpholino)ethanesulfonic acid.

strates, including ACh, inhibit their own catalysis at concentrations exceeding the K_m (≥1 mM, *i.e.* ≥20 × K_m for ATCh and mouse AChE (mAChE) (15)). AChE from *Drosophila*, but not from vertebrates, also shows substrate activation at low concentrations (23, 24). Competitive displacement, by ACh, of the specific PAS ligands, propidium and the peptidic toxin fasciculin, provides evidence that ACh binds the PAS in addition to the active site (10, 25, 26).

Electrostatic calculations based on the TcAChE structure and subsequent molecular dynamics simulation suggested that AChE may also have a "back door," distinct from the gorge entrance and whose transient opening would contribute to the high rate of traffic of substrates, products, and water into and out of the active center gorge (27, 28). Opening of this putative door would involve a displacement of the Trp^{86} side chain, which constitutes the thin wall separating the choline binding site in the active site from the outside solvent. Existence of residual catalytic activity of AChE complexes with the large fasciculin molecule, which binds the PAS to seal the gorge entrance (5, 18), may also argue for the need of an alternative entry portal(s) for the substrate (26, 29–31). Yet, crystal structures of fasciculin-AChE complexes did not reveal an open back door. To date, the functioning of the back door remains hypothetical and, apart from some speculation (32, 33), evidence for its existence has not been reported.

Although a structural perspective on the AChE catalytic mechanism should include the acylation and deacylation steps and related intermediates, the rapid substrate turnover precludes their entrapment and visualization in a crystalline state. Initial manual docking of an ACh molecule into the *Torpedo californica* (TcAChE) structure (4) was followed by structures of AChE complexes with competitive, reversible inhibitors (34–38), covalent organophosphate or carbamate inhibitors (39), bifunctional inhibitors (20, 32, 34, 40, 41), PAS inhibitors (5, 18, 19), and the substrate analogue, trimethylammoniotrifluoroacetophenone (TMTFA) (42). The latter provides a close structural mimic of the substrate-AChE tetrahedral transition state.

To enhance the opportunity of observing intact substrate molecules bound with high occupancies at the various sites, we expressed a catalytically inactive mAChE mutant, S203A, and crystallized it together with the wild type mAChE in a form that keeps potential ligand binding sites at the enzyme surface free of packing contacts (19, 20). We then soaked the crystals in concentrated solutions of the substrates ACh and acetylthiocholine (ATCh), the slowly hydrolyzable substrates succinyldicholine (SCh) and butyrylthiocholine (BTCh), the non-hydrolyzable substrate analogues TMTFA and 4-ketoamyltrimethylammonium (4K-TMA), and the reaction product choline (Scheme 1). The eight resulting crystalline complexes and conjugates, supported by binding and inhibition data, show complementary views of the transition state, the acyl-enzyme and the deacetylated enzyme, and substrate binding to the PAS. In addition, substrate binding sites remote from the active site and the PAS were identified. Hence these structures provide a comprehensive set of snapshots of the reaction intermediates along the gorge pathway and the likely modes of regulation by substrate binding to low affinity sites at the enzyme surface.

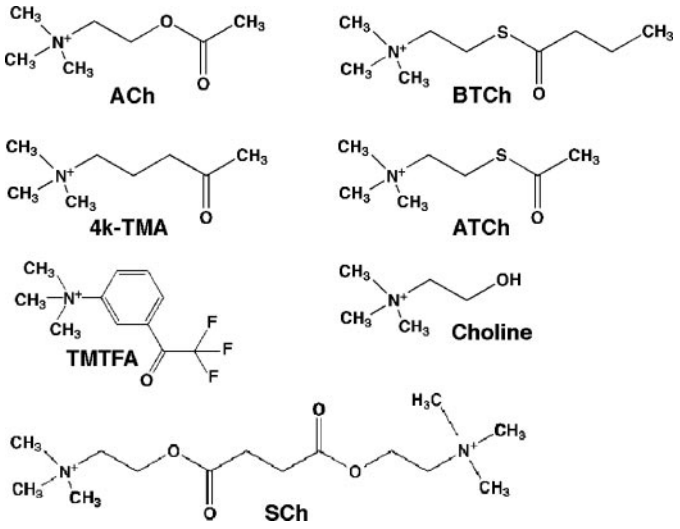

SCHEME 1. **The ligands used in this study.** Shown are the substrates ACh, ATCh, SCh, and BTCh, the substrate analogues TMTFA and 4K-TMA, and the reaction product choline.

MATERIALS AND METHODS

Chemicals—4K-TMA iodide was from ICN and ambenonium dichloride from Tocris Cookson. ACh, ATCh, SCh, BTCh, and choline, as chloride or iodine salts, were from Sigma. TMTFA iodide and decidium diiodide were respective gifts from Daniel M. Quinn, University of Iowa, Iowa City, UT, and Harvey A. Berman, State University of New York, Buffalo, NY. Polyethylene glycols were from Hampton Research, Fluka, or Sigma.

Enzymes—Soluble mAChE expressed in human embryonic kidney-293 cells (15, 43) was purified by affinity chromatography with elution using either 5 mM propidium diiodide (19) or 100 mM SCh dichloride; in the latter case, the eluted enzyme was immediately dialyzed to avoid precipitation/inactivation due to medium acidification through slow SCh hydrolysis. The mAChE mutant S203A was generated by site-directed mutagenesis, expressed in human embryonic kidney-293 cells, and purified using 100 mM decamethonium bromide (15, 43). The enzyme and mutant were extensively dialyzed against 1 mM Mes, pH 6.5, 1 M NaCl, 40 mM $MgCl_2$, 0.01% NaN_3 (w/v), and desalted by gel-filtration FPLC on Superdex-200 (Amersham Biosciences) in 1 mM Mes, pH 6.5, 50 mM NaCl, 0.01% NaN_3 (w/v) (crystallization buffer), or by extensive dialysis against this buffer. They were concentrated to about 10 mg/ml by ultrafiltration.

Crystallization, Complex Formation, and Data Collection—Crystallization was achieved at 4 °C by vapor diffusion using hanging drops (1–2 μl) and a protein-to-well solution ratio of 1:1, with P550MME or P600 (25–32%) (v/v) in either Hepes or sodium acetate (60–100 mM), pH 6.5–8.0, as the well solution (19). The TMTFA-mAChE complex was formed in solution using apo-mAChE at 5.0 mg/ml (~80 μM; 1.5 10^{10} × K_i (31)) and a 3-fold molar excess of the ligand over the enzyme, and concentrated prior to crystallization. The other seven complexes were generated by crystal soaking, carried out at 4 °C in sitting drops (20 μl) made of the well solution supplemented with the ligand (250 mM) and polyethylene glycol up to 35%

TABLE 1
Data collection and refinement statistics

	mAChE				S203A mutant			
	TMTFA	**4K-TMA**	**SCh**	**Choline**	**ACh**	**ATCh**	**SCh**	**BTCh**
Binding site(s)	AS[a]	AS/PAS	AS/PAS	AS/PAS	AS/PAS	AS/PAS/BDR	AS/PAS/BDR	PAS
Panel in Fig. 2	*A*	*B*	*F*	*H*	*C*	*D*	*E*	*G*
Data collection[b]								
Beamline (ESRF)	ID14-EH1	ID14-EH1	ID14-EH4	ID14-EH4	ID14-EH2	ID14-EH4	ID14-EH4	ID14-EH2
Wavelength (Å)	0.933	0.933	0.975	0.975	0.933	0.975	0.975	0.933
Resolution range (Å)	20–2.4	30–2.2	30–2.05	30–2.25	30–2.55	30–2.15	30–2.25	20–2.65
Observations	276,837	351,519	327,048	302,093	259,660	363,316	337,398	231,897
Unique reflections	78,296	102,641	112,415	92,590	65,686	98,802	89,067	57,849
Multiplicity	3.5 (3.6)	3.4 (3.3)	2.9 (1.7)	3.3 (2.5)	3.9 (3.9)	3.7 (3.1)	3.8 (3.1)	4.0 (4.0)
Completeness (%)	99.4 (99.5)	100 (98.9)	90.1 (55.1)	96.2 (96.2)	99.9 (99.9)	96.9 (96.9)	95.4 (69.4)	99.9 (99.9)
$I/\sigma(I)$	11.3 (3.3)	11.9 (2.8)	10.6 (1.4)	11.9 (3.0)	15.2 (4.3)	13.0 (3.4)	14.3 (3.1)	16.0 (4.0)
R_{merge}[c]	8.2 (44.7)	6.5 (45.1)	6.1 (38.5)	7.3 (33.8)	6.8 (42.4)	6.2 (38.3)	5.6 (48.7)	6.8 (46.7)
Wilson plot B-factor (Å^2)	52.6	41.1	35.3	41.7	42.3	35.1	51.3	49.2
Refinement								
R_{cryst}[d]/R_{free} (%)	18.6/21.4	18.3/21.7	19.2/22.1	17.5/19.8	18.9/22.4	17.7/20.9	17.8/19.9	19.9/24.2
R.m.s. deviation[e]								
Bonds (Å)/Angles (°)	0.01/1.29	0.01/1.28	0.01/1.41	0.01/1.26	0.01/1.30	0.01/1.23	0.01/1.37	0.01/1.24
Chiral volume (Å^3)	0.095	0.097	0.112	0.075	0.091	0.074	0.081	0.086
Average B-factor (Å^2)								
Main/side chains	65.4 (66.4)	57.6/58.9	58.2/59.4	52.9/54.1	38.8/39.6	56.7/57.8	49.8/51.3	46.2/47.5
Solvent/carbohydrate-PEG	63.0/87.3	59.6/64.5	62.5/72.7	52.9/82.5	37.2/57.3	64.2/83.6	50.5/61.2	39.5/42.8
Ligand (AS/PAS/BDR)*	57.6/−/−	49.6/74.2/−	83.8/−/−	81.3/87.3/−	52.6/55.3/−	76.4/87.2/80.4	77.7/−/77.3	66.8/85.3/−
Main/side chain ΔB for bonded atoms (Å^2)	0.93/1.34	0.94/1.48	0.98/1.52	0.72/1.23	0.86/1.43	0.82/1.33	0.85/1.44	1.07/1.72
PDB accession code	2H9Y	2HA0	2HA2	2HA3	2HA4	2HA5	2HA6	2HA7

[a] AS, active site; PAS, peripheral anionic site; BDR, back door region.
[b] Values in parentheses are those for the last shell.
[c] $R_{merge} = \Sigma_{hkl} \Sigma_i |I_{i(hkl)} - \langle I_{hkl} \rangle| / \Sigma_{hkl} \Sigma_i I_{i(hkl)}$, where I is an individual reflection measurement and $\langle I \rangle$ is the mean intensity for symmetry-related reflections.
[d] $R_{cryst} = \Sigma_{hkl} \| F_o| - |F_c| \| / \Sigma_{hkl} |F_o|$, where F_o and F_c are observed and calculated structure factors, respectively. R_{free} is calculated for 2% of randomly selected reflections excluded from refinement
[e] Root mean square deviations from ideal values.

(~0.6 M) to ensure cryoprotection; the soaking drops were renewed twice at 12-h intervals and again just before direct crystal flash-cooling in the nitrogen gas stream. Crystals belong to the orthorhombic space group $P2_12_12_1$ with unit cell dimensions $a = 79$ Å, $b = 112$ Å, $c = 227$ Å. Oscillation images were integrated with DENZO (44) and data were scaled and merged with SCALA (45) (Table 1).

Structure Determination and Refinement—The apo-mAChE structure (Protein Data Bank entry 1J06 (19)) without solvent was used as a starting model to refine the reported structures with REFMAC (46) using the maximum likelihood approach and incorporating bulk solvent corrections, anisotropic F_{obs} *versus* F_{calc} scaling and TLS refinement with each subunit defining a TLS group (Table 1). Typically, rigid-body refinement was first performed on each of the two subunits forming the crystalline mAChE dimer (19) using all data followed by cycles of restrained refinements. Random sets of reflections were set aside for cross-validation purposes. For each structure, the resulting σA-weighted $2F_o - F_c$ and $F_o - F_c$ electron density maps were used to position the ligand. Automated solvent building was performed with ARP/wARP (47) and manual adjustment with the graphics program TURBO-FRODO (66) and COOT (48).

The final structures, one apo-S203A and eight S203A or mAChE complexes, comprise residues Glu^1–Thr^{543} and Glu^4–Thr^{543} for the two mAChE/S203A molecules in the asymmetric unit, respectively, and GlcNAc moieties linked to Asn^{350} and Asn^{464}. High temperature factors and weak electron densities are observed for residues within the surface loop region Asp^{491}–Pro^{498}. The average root mean square (r.m.s.) deviation value between the nine structures and the apo-mAChE structure is 0.24 Å for 535 Cα atoms (from 0.19 Å for the SCh-mAChE complex to 0.294 Å for the 4K-TMA-mAChE complex). The stereochemistries of the structures were analyzed with PROCHECK (49); with the exception of residue Ser/Ala^{203}, no residues were found in the disallowed regions of the Ramachandran plot. The atomic coordinates and structure factors of the four S203A (ACh, ATCh, SCh, and BTCh) and four mAChE complexes (TMTFA, 4K-TMA, SCh, and choline) have been deposited with the RCSB Protein Data Bank (Table 1). Figures were generated with PyMOL (50).

Inhibition and Binding Studies—Inhibition by SCh, 4K-TMA, and choline of mAChE-catalyzed ATCh hydrolysis was measured spectrophotometrically (51) in 0.1 M phosphate buffer, pH 7.0, at 22 °C. The inhibition constants, K_i and αK_i, were determined from the dependence of slopes and y intercepts of Lineweaver-Burk plots on inhibitor concentration (15).

Binding of ligands ACh, ATCh, SCh, BTCh, 4K-TMA, and choline to mAChE (200 nM) and the S203A mutant (100 nM) was measured from the dependence of the pseudo-first order association rate, k_{obs}, of the reversible bisquaternary inhibitors ambenonium (2 or 5 μM) (52) or decidium (1 μM) (53) on ligand concentration (from 1 μM to 30 mM for 4K-TMA and to 300 mM for the other ligands). Rates were monitored in a millisecond time frame by stopped-flow measurements of intrinsic Trp fluorescence quenching of mAChE or its mutant as

described (54). Dissociation constants, K_d, were determined from semi-logarithmic plots of k_{obs} *versus* ligand concentration ([*L*]) and calculated by nonlinear regression using Equation 1,

$$k_{obs} = k_{obs}^{0}/(1 + [L]/K_d) \quad \text{(Eq. 1)}$$

where k_{obs}^{0} is the pseudo-first order rate constant for ambenonium or decidium association in the absence of ligand. When k_{obs} *versus* [*L*] plots were biphasic, two dissociation constants, K_d and K_d^L, characterizing ligand binding to the enzyme and the enzyme-ligand complex, respectively, were calculated using Equation 2,

$$k_{obs} = (k_{obs}^{0} - k_{obs}^{L,0})/(1 + [L]/K_d) + k_{obs}^{L,0}/(1 + [L]/K_d^L) \quad \text{(Eq. 2)}$$

where $k_{obs}^{L,0}$ is the limiting first-order rate constant for competitor association with the enzyme-ligand complex.

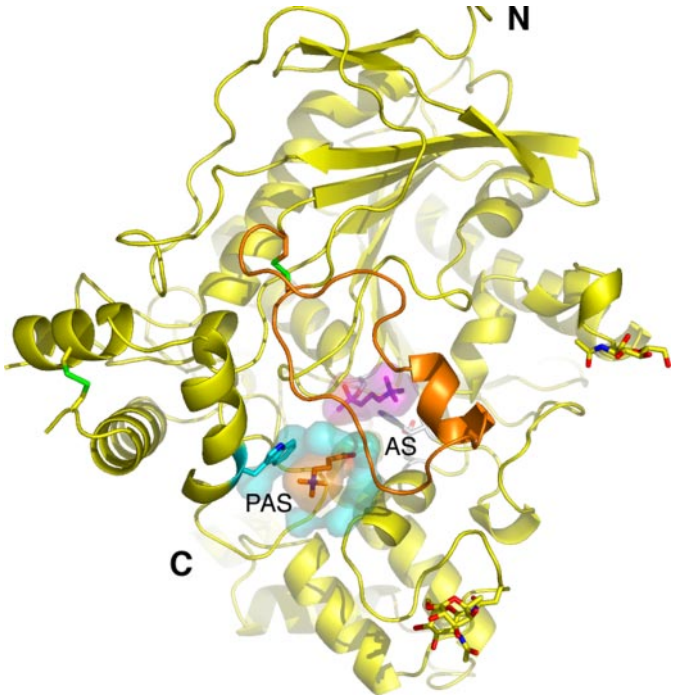

FIGURE 1. **Overall view of the mAChE subunit.** mAChE is viewed down into the gorge with one 4K-TMA molecule (*magenta* atoms and surface) bound in the active site (labeled *AS*) and a second 4K-TMA molecule (*orange* atoms and surface) bound at the PAS (*blue* Trp[286] and surface). The long Ω loop Cys[69]–Cys[96] is in *orange* and the disulfide bounds in *green*. The GlcNac moieties linked to Asn[350] on same face as the gorge entrance (*bottom*) and Asn[464] in the back door region (*right*) are shown with *red* oxygens and *blue* nitrogens. N and C termini are indicated.

RESULTS AND DISCUSSION

Procedures for Trapping Intact Substrate in the Crystalline Enzyme

The 2.65-Å resolution structure of the S203A mutant, compared with apo-mAChE (r.m.s. deviation value: 0.26 Å for 535 Cα atoms), shows an undisrupted catalytic site architecture despite the absence of the Ser hydroxyl, as well as unaltered topography for the PAS region (Fig. 1). Soaking a S203A crystal with 50 mM ATCh ($\sim 10^3 \times K_m$ and $4 \times K_{ss}$ for mAChE; $\sim 50 \times K_d$ for the mutant; Table 2) led to a 2.25-Å resolution structure in which only the reaction products thiocholine (TCh) and acetate were found, well ordered and with high occupancy, in the active center gorge (not shown). Despite the small size of choline, the side chain of Tyr[337], located in the constricted region of the gorge, was found rotated by 24° and tilted by 35° compared with its position in apo-mAChE, a movement that increases the gorge internal diameter and may favor choline release in catalysis. Subsequent analyses of a choline-S203A and a choline-mAChE complex, both formed with 50 mM choline ($15–50 \times K_d$; Table 2), showed bound choline molecules in the same position and orientation as the bound TCh (not shown). This not only indicates that the thioester bond in the substrate trapped in the S203A crystal was cleaved by the synchrotron radiation during data collection, but also that absence of the Ser[203] hydroxyl does not alter orientation of the choline moiety, despite the 4–10-fold lower affinities of the mutant for

TABLE 2

Constants for ligand interaction with mAChE and the S203A mutant

All values are means ($n = 3$) of individual data (±S.D.).

Ligand	Enzyme	Inhibition constants (K_i)[a]	Binding constants (K_d and K_d^L)[b]				Direct titration, (K_d)	Catalytic constants (K_m and K_{ss})[c]	Panel in Fig. 2
			Ambenonium kinetics		Decidium kinetics				
			K_d	K_d^L	K_d	K_d^L			
		mM	mM	mM	mM	mM	mM	mM	
ACh	mAChE		0.054 (±0.011)	3.6 (±1.4)	0.079 (±0.049)	5.6 (±1.8)			
	S203A		2.0 (±0.2)	ND[d]	NM[e]	NM	1.7 (±0.7)		*C*
ATCh	mAChE		0.046 (±0.023)	1.3 (±0.7)	0.16 (±0.10)	3.0 (±0.5)		K_m, 0.046, K_{ss}, 12	
	S203A		0.62 (±0.06)	ND	1.2 (±0.2)	ND			*D*
SCh	mAChE	0.021 (±0.002)	NM	NM	0.022 (±0.001)	ND			*F*
	S203A		0.048 (±0.004)	ND	NM	NM			*E*
BTCh	mAChE		0.23 (±0.04)	ND	0.28 (±0.05)	ND		K_m, 0.093; K_{ss}, 7.1	
	S203A		0.44 (±0.05)	ND	0.76 (±0.32)	ND			*G*
4K-TMA	mAChE	0.023 (±0.006)	0.037 (±0.013)	ND	0.033 (±0.02)	8.4 (±4.5)			*B*
	S203A		0.86 (±0.11)	ND	NM	NM			
Choline	mAChE	1.4 (±0.2)	0.93 (±0.12)	ND	NM	NM			*H*
	S203A		3.4 (±0.2)	ND	NM	NM			

[a] The corresponding αK_i constants, more than 1 order of magnitude higher than the K_i values, are not reported.
[b] Determined by nonlinear regression using equations 1 and 2 (*cf,* "Materials and Methods" and Fig. 5).
[c] The Michaelis (K_m) and substrate inhibition constants (K_{ss}) are from Refs. 15 and 64.
[d] ND, not detectable.
[e] NM, not measured.

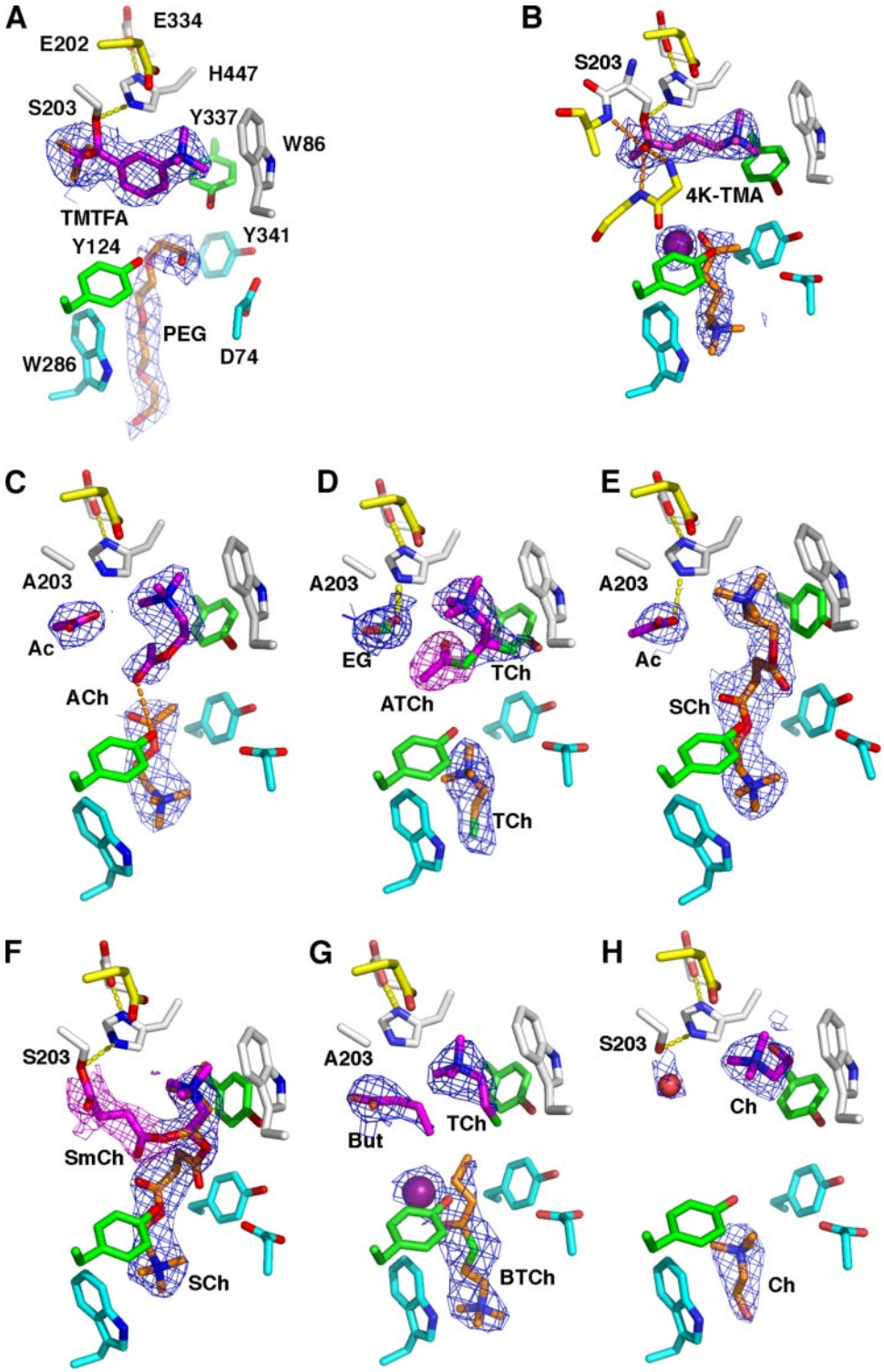

FIGURE 2. **Ligand binding in the active center and at the peripheral site.** Close-up views of mAChE bound with TMTFA (and polyethylene glycol) (*A*) and 4K-TMA (and iodide, as a *magenta sphere*) (*B*), the S203A mutant bound with ACh (and acetate) (*C*), ATCh (and TCh and ethylene glycol) (*D*), and SCh (and acetate) (*E*), mAChE bound with SCh (and succinylmonocholine, labeled SmCh) (*F*), the S203A mutant bound with BTCh (and butyrate, TCh and iodide) (*G*), mAChE bound with choline (and water, as a *red sphere*) (*H*). The side chains of Ser/Ala^{203}, Glu^{334}, His^{447}, and Trp^{86} in the active site pocket are shown in *white* and that of Glu^{202} in *yellow*; those of Tyr^{124} and Tyr^{337} in the constricted region of the gorge are in *green*; and those of Trp^{286}, Tyr^{341}, and Asp^{74} in the PAS in *cyan*. The nitrogen, oxygen, and sulfur atoms are in *blue*, *red*, and *green*, respectively. Both the *blue* and *fushia* $2F_o - F_c$ σA-weighted electron density maps are contoured at 1.2 σ.

ATCh and choline (Table 2). To increase the probability of observing intact substrate molecules bound with high occupancies, we employed concentrations greater than the substrate inhibition constants (250 mM, *i.e.* $\sim 20 \times K_{ss}$ for ACh and mAChE; higher concentrations led to ill-diffracting crystals), and substrates or analogues with oxo or keto bonds expected to be less sensitive to radiation (Scheme 1).

Determination and Quality of the Structures

The structures of mAChE in complexes with the ACh keto analogues, TMTFA and the isosteric 4K-TMA, the poor substrate SCh, and the product choline, and those of the S203A mutant in complexes with substrates ACh and ATCh and poor substrates SCh and BTCh, were solved by difference Fourier methods and refined in the 2.05–2.65-Å resolution range, with good *R*-factor values and stereochemistries (Table 1). For all eight complexes, the excellent quality of the final electron density maps permits an unambiguous positioning of the ligands, which are well ordered and bound with high occupancy. The polypeptidic chain, which folds into a 12-stranded central-mixed β-sheet surrounded by 14 α-helices, adopts the same conformation as found in the apo-mAChE and S203A structures (r.m.s. deviation values in the 0.19–0.29 Å range for 534 Cα atoms). This indicates that major conformational changes are not associated with ligand binding. Only a rotation, up to 26°, and a tilt, up to 50°, of the Tyr^{337} side chain is observed throughout, which may simply reflect the high mobility of this residue in the crystaline state (19, 20, 55). Hence, these structures, when complemented by kinetic analyses performed on the same complexes, provide a comprehensive set of snapshots for exploring the routes for trafficking of substrate into

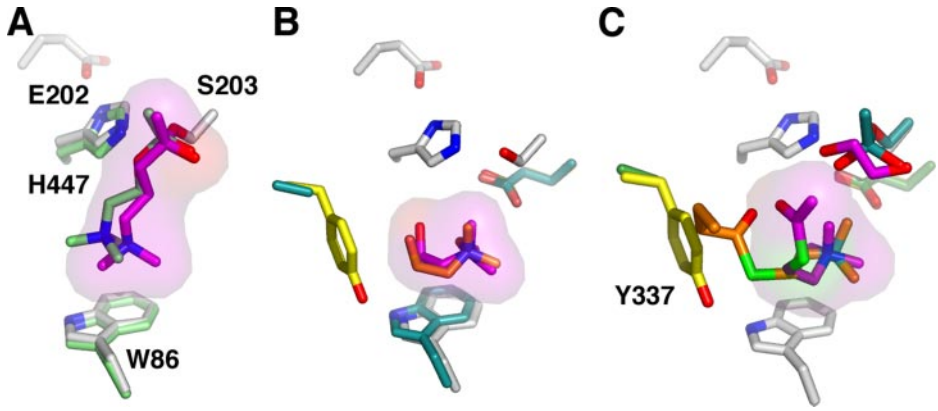

FIGURE 3. **Comparison of active site-bound ligands.** Overlays of 4K-TMA bound to mAChE (*magenta* molecule and surface) with ACh (*green*) docked in TcAChE (PDB entry 2ACE) (*A*), choline bound to mAChE (*magenta* molecule and surface) with choline bound to BChE (*orange*) (entry 1P0M), (*B*), ATCh bound to the S203Ala mutant (*magenta* molecule and surface) with BTCh (*orange*) and soman (*blue*) bound to BChE (entry 1P0P) (*C*). Note the Tyr337Ala mutation in BChE.

and product of the active center gorge, as well as the location of alternative substrate binding sites at the enzyme surface.

Substrate and Product Binding in the Active Site and at the Peripheral Anionic Site

TMTFA-mAChE Complex—The structure of the co-crystallized TMTFA-mAChE complex shows the substrate analogue oriented perpendicular to the gorge axis and positioned within covalent bond distance of the Ser^{203} hydroxyl in the active site at the base of the gorge (Fig. 2*A*). The trimethylammonio group is ideally positioned for cation-π interaction with the 6-membered ring of Trp^{86}, located 4.2 Å away. The carbonyl, which points into the oxyanion hole, is hydrogen bonded to Ala^{204} and the $Gly^{121/122}$ backbone amines, whereas the trifluoromethyl group is anchored within the acyl pocket, bordered by Trp^{236}, Phe^{295}, Phe^{297}, and Phe^{338}. This position and orientation of the bound TMTFA are consistent with those found in the TMTFA-TcAChE complex (42) (r.m.s. deviation value: 0.8 Å for 518 Cα atoms). A well defined polyethylene glycol molecule (arising from the crystallization liquor) is bound at the PAS in a similar position as in apo-mAChE (19). Hence, this structure provides a frame of reference for specific *versus* nonspecific ligand binding at the PAS, both altering the shape of the electron density maps.

4K-TMA-mAChE Complex—In the 4K-TMA-mAChE complex, two well ordered molecules of the substrate analogue are, respectively, bound in the active site, and at the PAS at the gorge entry (Fig. 2*B*). The 4K-TMA bound in the active site, oriented as is TMTFA bound at the same site (*cf.* Fig. 2*A*), adopts a near perfect non-relaxed *trans*, *trans* conformation. The carbonyl carbon is within covalent bond distance (1.39 Å) of the Ser^{203} hydroxyl, whereas the trimethylammonio group faces (4.2 Å) the six-membered ring of the Trp^{86} indole. The position and conformation of 4K-TMA in the mAChE active site resembles those of the ACh molecule manually docked into the active site of TcAChE (4), but the quaternary (cationic alkyl) ammonium group deviates by 1 Å from its position in docked ACh as to face the five-membered ring of the Trp^{286} indole (Fig. 3*A*). This distinctive position also coincides with that of the corresponding atoms of TMTFA bound to mAChE (*cf.* Fig. 2*A*). The tetrahedral conformation of the 4K-TMA carbonyl carbon, along with its short distance to the Ser^{203} hydroxyl, indicates that a perfect tetrahedral hemiketal conjugate was generated and trapped in the crystalline enzyme.

The 4K-TMA molecule bound at the PAS surface aligns along the gorge axis and adopts the same non-relaxed *trans*, *trans* conformation as in the active site, except for maintaining a trigonal, planar instead of tetrahedral configuration (Fig. 2*B*). The quaternary ammonium group establishes cation-π interaction (4.4 Å) with the Trp^{286} indole and van der Waals contacts (4 Å) with Tyr^{72} at the gorge entrance. The keto moiety, positioned between Tyr^{124} and Tyr^{341} deeper in the gorge, has its carbonyl oxygen linked to the Phe^{295} backbone nitrogen atom via a 2.6-Å distant iodide ion (the added counter ion to 4K-TMA), and with the residue pair Asp^{74}/Tyr^{341} on one side and its methyl in van der Waals contacts with Tyr^{124} on the other side. Hence the PAS-bound 4K-TMA is inverted with respect to the dipole moment of the gorge.

Comparison of the 4K-TMA-mAChE complex with apo-mAChE (r.m.s. deviation value: 0.27 Å for 533 Cα atoms) shows limited conformational changes associated with 4K-TMA binding (not shown). Some side chains reorient, such as those of Tyr^{341} and Asp^{74} at the PAS, which move slightly into the gorge, and of Tyr^{337}, which rotates by ~8° to enlarge the gorge diameter near its constricted region, along with small movements of Trp^{86} (~4°) in the choline binding site and Trp^{286} (~17°) at the PAS. A subtle rotation, by 18°, of the Ser^{203} hydroxyl helps position the tetrahedral conjugate to optimize occupation of the oxyanion hole.

Kinetics studies show that 4K-TMA is a reversible, non-hydrolyzable substrate analogue with lower affinity for the S203A mutant than for mAChE (Table 2). In fact, soaking of 4K-TMA in the S203A crystal led to a structure devoid of a bound ligand (not shown), consistent with the role of Ser^{203} for stabilizing the analogue as a tetrahedral hemiketal within the intact active center of mAChE. However, the basis for the absence of bound 4K-TMA at the PAS of the mutant is unclear.

Acetylcholine- and Acetylthiocholine-S203A Complexes—In the ACh-S203A complex, two well ordered ACh molecules are found in the active site and at the PAS, respectively (Fig. 2*C*). The ACh positioned in the active site adopts a relaxed *trans*, *gauche* conformation, consistent with the most stable conformation of ACh seen by crystallography and NMR spectroscopy (56, 57). This bound ACh has its quaternary ammonium group facing Glu^{202} (4.1 Å) and in a cation-π interaction with the 6-membered ring of Trp^{86} (4.3 Å), whereas the acetoxy moiety, located near the constricted region of the gorge, interacts via

the oxygen with Tyr^{124} on one side of the gorge and, via the methyl, with Tyr^{337} and Phe^{338} on the other side. An acetate molecule (arising from the crystallization liquor) occupies the oxyanion hole, as do carbonate or acetate molecules found in previous mAChE structures (19).

ACh bound at the PAS adopts a position and a non-relaxed *trans*, *trans* conformation similar to those of 4K-TMA bound at the same site (Fig. 2*C*, and *cf.* Fig. 2*B*). As a result, the PAS-bound ACh is inverted with respect to the molecule bound in the active site, such that the two acetyl groups are separated by only 4.5 Å in the constricted region of the gorge. These two ACh orientations at the PAS and at the base of the gorge may reflect two successive snapshots of ACh trafficking into the gorge. The orientation of the PAS-bound substrate may also limit its entry to the active center, when inhibition of catalysis by excess substrate occurs. The largest differences compared with apo-mAChE are confined to a ~20° rotation of the Tyr^{337} phenol that increases the gorge diameter at mid-point and a ~10° rotation of Trp^{286} that enlarges the gorge entrance.

In the ATCh-S203A complex (Fig. 2*D*), near equal amounts of intact ATCh, in a relaxed *trans*, *gauche* conformation as seen in the ACh-S203A complex (*cf.* Fig. 2*C*), and of TCh (arising from partial cleavage of the thioester bond during data collection) are bound in the catalytic site, whereas an ethylene glycol molecule (arising from the crystallization liquor) occupies the oxyanion hole. A second TCh molecule (presumably, also generated in the active center during data collection) is bound at the PAS. In the active site, the overlapped choline moieties in the substrate and product face Glu^{202} (4.2 Å) and are in a cation-π interaction with the nearly parallel Trp^{86} indole. The position of the free sulfhydryl in TCh creates unfavorable interactions with the Tyr^{337} hydroxyl (2.1 Å) and Trp^{286} indole (3.2 Å). Compared with apo-mAChE, a 25° rotational movement of Tyr^{337} enlarges the gorge in the region of constriction (not shown). The presence of a non-attributed electron density with peaks above 4.5 σ near the Tyr^{337} phenol ring and negative peaks for the tip of this ring indicate even higher mobility of Tyr^{337} in this complex than in the others. The overlay of ATCh-bound S203A with BTCh-bound soman-inhibited butyrylcholinesterase (BChE) (58) (r.m.s. deviation value: 0.87 Å for 500 Cα atoms) reveals a common substrate orientation dictated by the position of the quaternary ammonium groups, anchored near Trp^{86}, whereas the two acyl chains diverge by 90° due to the Y337A substitution in BChE (Fig. 3*C*). At the PAS, the bound TCh, inverted with respect to the PAS-bound 4K-TMA in mAChE and ACh in the mutant (*cf.* Fig. 2, *B* and *C*), establishes similar cation-π interactions associated with side chain repositioning as in the other complexes.

Succinylcholine-S203A and -mAChE Complexes—The structures of the S203A mutant and mAChE in complexes with the poor, slowly deacylating substrate SCh (Table 2) are similar to each other (Fig. 2, *E* and *F*). Both show a symmetrical SCh molecule that spans the full-length of the gorge with its two choline moieties, respectively, bound into the anionic subsite of the active center and at the gorge entrance. These moieties resemble, in their positions and conformations, those of the two inverted ACh molecules bound to the S203A mutant (*cf.* Fig. 2*C*). SCh binding is associated with a loop-forming bend of the succinate moiety, resulting in a S-shaped conformation for SCh. The two central succinyl carbonyls are tilted by ~127° compared with 180° in an extended *trans* conformation. This conformation facilitates cation-π interactions of the two distant SCh quaternary ammonium groups with the Trp^{286} and Trp^{86} indole rings, respectively, in the PAS and the choline binding subsite of the active center. The binding interactions are dominated by van der Waals contacts with the apolar side chains that line the gorge (Phe^{297}, Tyr^{337}, Phe^{338}, and Tyr^{341}), whereas a few polar interactions, mediated by solvent molecules, involve one carbonyl oxygen of the succinyl moiety and the Tyr^{124} hydroxyl and Asp^{74} carboxylate. The major conformational differences compared with apo-mAChE involve the side chain of Tyr^{337}, which rotates by 26° and is tilted by 68°, and that of Trp^{286} that moves by 9°. The drastic rotation of Tyr^{337} promoted by the bound succinyl moiety induces a significant increase, by ~2.3 Å, of the gorge diameter. These displacements suggest that similar enlargements occur in solution facilitating substrate/product trafficking within the gorge.

In the SCh-mAChE complex, but not the SCh-S203A complex, a bifurcated electron density deviating from that accounting for the deepest SCh ether oxygen is clearly visible near the catalytic site (Fig. 2*F*). Perfect filling of this density by a succinylmonocholine molecule anchored to the catalytic Ser^{203}, and oriented as are TMTFA and 4K-TMA bound to mAChE (*cf.* Fig. 2, *A* and *B*), reveals that an succinyl-enzyme intermediate (distance of 1.6 Å from the Ser hydroxyl to the succinylmonocholine carbonyl carbon) was trapped in the crystal, in near-equal amounts as intact SCh and with overlapping choline moieties proximal to Trp^{86}. Entrapment of an acyl-enzyme intermediate in crystalline mAChE suggests that, compared with ACh, the slower rate of SCh hydrolysis (Table 2) may reflect a slower rate of acylation and/or deacylation. In the SCh-S203A complex, an acetate molecule (arising from the crystallization liquor) is bound within the oxyanion hole in a position that roughly coincides with that of the acyl moiety attached to Ser^{203} in the SCh-mAChE complex (Fig. 2, *E* and *F*).

Butyrylthiocholine-S203A Complex—Hydrolysis of BTCh catalyzed by mAChE is about 100 times slower than that of ACh or ATCh despite only 4-fold lower K_d and 2-fold lower K_m values (Table 2). The structure of the S203A mutant in complex with BTCh shows a butyrate and a TCh molecule (both arising from cleavage of the thioester bond during data collection) bound in the catalytic site and an intact BTCh molecule bound at the PAS (Fig. 2*G*). In the catalytic site, TCh adopts the same position as in the ATCh-S203A complex (*cf.* Fig. 2*D*), whereas the butyrate occupies the oxyanion hole, as do acetate and ethylene glycol in other structures (*cf.* Fig. 2, *C–E*). Overlay of this structure with that of butyrate-bound BChE (58) (r.m.s. deviation value: 0.9 Å for 503 Cα atoms) shows the butyryl chain oriented perpendicular to its position in BuChE due to differences in the shape of the acyl pocket between the two enzymes.

The BTCh molecule bound at the PAS adopts a position and a non-relaxed *trans, trans* conformation similar to those of 4K-TMA, ACh, and ATCh bound at the same site (*cf.* Fig. 2, *B–D*, and *G*). The quaternary ammonium is oriented toward the gorge entrance. The butyryl moiety, anchored 2.8 Å deeper

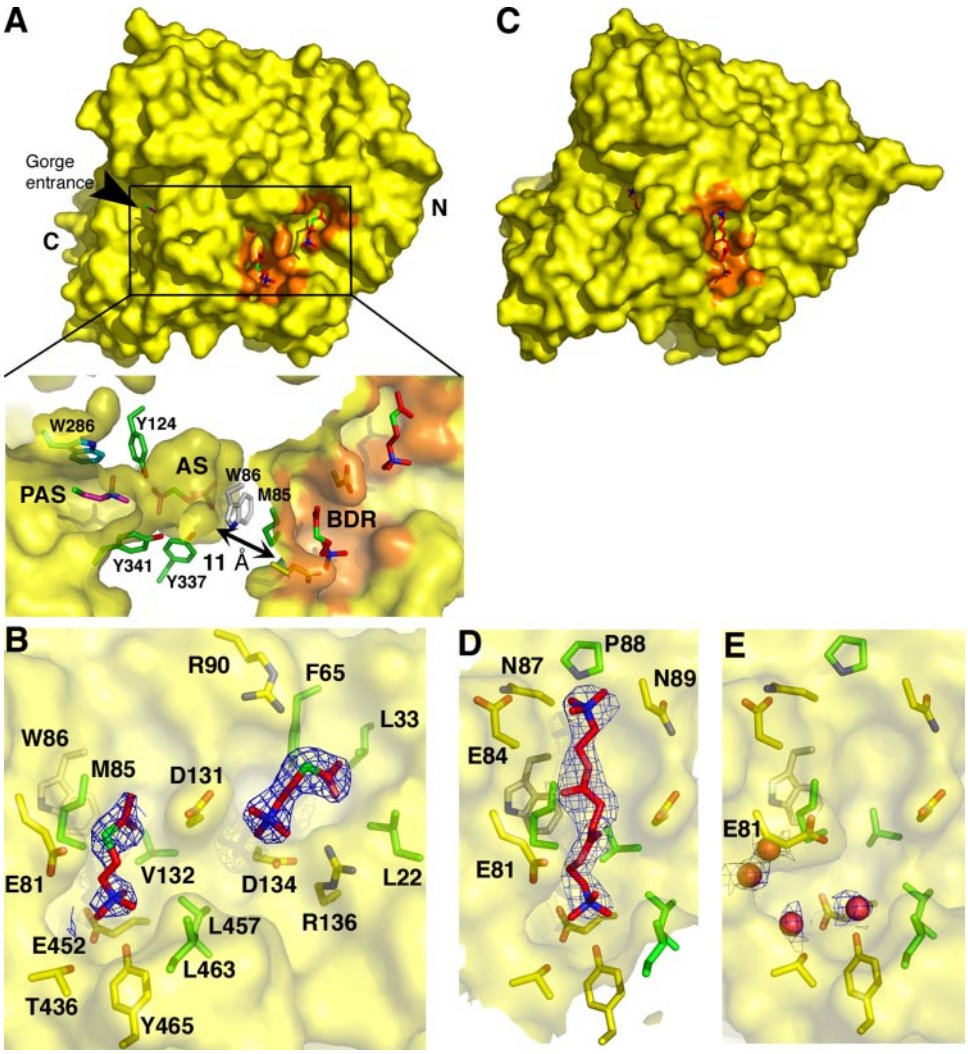

FIGURE 4. **Substrate binding to the surface in the back door region.** Overall and close up views of the two ATCh (*A* and *B*) and one SCh molecules (*C* and *D*) (*red* carbon atoms) bound in the putative back door region of the S203A mutant. The molecular surfaces buried by the bound ligands are highlighted in *orange*. The nitrogen, oxygen, and sulfur atoms in the ligands are in *blue*, *red*, and *green*, respectively. On *panel A, C*, the ligands bound at the gorge entrances (*cf.* Fig. 2, *D* and *E*) are partly visible. The *inset below panel A* displays a clipped surface through the thin portion of the gorge wall near Trp[86], highlighting the close proximity of the ATCh molecules respectively bound in the active site (labeled *AS*) and the back door region (*BDR*). The electron density maps in *panels B* and *D* are contoured at 1.2 σ. *E*, the back door region with bound water molecules (*red* and *orange spheres*) as seen in the SCh-mAChE complex. Note the flip of the Glu[81] side chain associated with ligand binding.

in the gorge than the acetyl moiety of ATCh (*cf.* Fig. 2*D*), is in the stacking interaction with Tyr[341], whereas its carbonyl oxygen is linked to the Phe[295] backbone amide nitrogen via a 2.75-Å distant iodide ion (the added counter ion to BTCh), similarly as found in the 4K-TMA-mAChE complex. Again, a 17° rotation of Tyr[337] enlarges the diameter in the constricted region of the gorge.

The presence of intact BTCh at the PAS, but not in the active center of the S203A mutant, suggests that the lower affinity of the mutant for BTCh is entirely due to absence of the Ser[203] hydroxyl (Table 2). This also suggests that the *trans*, *gauche* conformation of the substrates in the active center (*cf.* Fig. 2, *C* and *D*) is more sensitive to radiation than the *trans*, *trans* conformation adopted at the PAS (*cf.* Fig. 2, *B*, *C*, and *G*).

Choline-mAChE Complex—The structure of mAChE bound with the reaction product shows two choline molecules, respectively, bound near the catalytic site and at the PAS (Fig. 2*H*). At the active center, the choline quaternary ammonium group faces Glu[202] (3.9 Å) and establishes a cation-π interaction (4.3 Å) with the six-membered ring of Trp[86], with the three methyls oriented nearly parallel to the indole ring. The primary alcohol carbon is in van der Waals contact with the Tyr[337] phenol, which is oriented perpendicular to Trp[86], whereas the oxygen is bound to the His[447] backbone carbonyl oxygen. In the oxyanion hole, a water molecule is bound to the Ser[203] hydroxyl and occupies the same position as the acetate, ethylene glycol, or butyrate found in other structures (*cf.* Fig. 2, *C–E* and *G*). The overlay of the choline-mAChE and choline-BChE (58) complexes (r.m.s. deviation value: 0.95 Å for 501 Cα atoms) shows similarly oriented bound choline molecules with their quaternary ammonium groups separated by only 0.25 Å near the acyl pocket and overlapping primary alcohols directed toward the gorge entrance (Fig. 3*B*). This orientation of the bound choline, compared with bound ACh or ATCh in the S203A mutant (*cf.* Fig. 2, *C* and *D*), argues for a ~90° flip of the choline product upon dissociation before it leaves the gorge.

At the PAS, the choline quaternary ammonium group establishes cation-π interaction with Trp[286] (4.4 Å) and van der Waals contact with Tyr[124] and Tyr[341], whereas the oxygen atom points outside the gorge and establishes a weak (long range) hydrogen bond with the Tyr[72] hydroxyl (Fig. 2*H*). Hence, in contrast to the PAS-bound substrates, PAS-bound choline and TCh are aligned with the dipole moment of the gorge (Fig. 2, *D* and *H*). This orientation, along with the limited inhibition of mAChE by choline (Table 2), suggests that this choline/TCh molecule reflects the egressing product, exiting from the gorge.

Substrate Binding at Surface Sites Removed from the Gorge Entrance

At the molecular surfaces of the SCh- and ATCh-S203A complexes, strong electron densities with peaks above 4 σ (SCh-S203A complex) and 3.7 σ (ATCh-S203A complex) unambiguously account for one SCh and two ATCh molecules

bound far from the gorge entry, in the region of the putative back door (Fig. 4).

In the two complexes, one substrate molecule occupies a depression delimited by helix $\alpha\beta$3,2 and the $\alpha\beta$3,2-β2 segment in the long Ω loop, Cys^{69}–Cys^{96}, on one side, the loop connecting helix α(1)8,9 to helices α(2)8,9 and α(2)8,9 on the other side, and loop β3-α3,4 at the edge and loop β8-α(1)8,9-α(1)8,9 at the base (Fig. 4, *A* and *C*). The choline moieties common to the bound ATCh and SCh are similarly positioned at the base of the depression, whereas the second choline moiety in SCh extends toward the top (Fig. 4, *B* and *D*). The succinate moiety of SCh adopts a more extended conformation (105° instead of 126°) than that of SCh bound within the gorge, resulting in inter-ammonium distances of 12.8 and 11 Å, respectively. The interaction is dominated by van der Waals interactions primarily with sequence-conserved residues from the long Ω loop, arguing for a key role of this surface loop for AChE activity as earlier proposed from fluorescence (59–61) and molecular modeling studies (62). Indeed, the side chains of Glu^{81}, Glu^{84}, Met^{85}, and of the Asn^{87}-Pro^{88}-Asn^{89} tripeptide in the long Ω loop, along with that of Asp^{131} in the β3-α3,4 loop, interact with the acetyl group in ATCh and an acyl group in SCh, whereas the side chains of Thr^{436} in the β8-α(1)8,9 loop, Glu^{452} in helix α(1)8,9, and Leu^{457} and Tyr^{465} in loop α(1)8,9-α(2)8,9 complete the binding site for the choline moiety. Several aliphatic residues, such as Pro^{88} and Val^{132} at the top and Leu^{463} at the base, complete the shape of the cavity. It is worth noting that four conserved negatively charged residues (Glu^{81}, Glu^{84}, Asp^{131}, and Glu^{452}) are involved in SCh binding (*versus* two for ATCh binding), and that the conserved pair Tyr^{465}/Glu^{452}, located near the quaternary ammonium group of either substrate, is reminiscent of the functional Tyr^{72}/Asp^{74} pair located within the PAS. The ~10 Å distance between this surface binding site and the conserved Asn^{464}-linked carbohydrate moiety excludes direct contribution of this carbohydrate moiety for ligand binding.

In the ATCh-S203A complex, the second substrate molecule bound at the surface in the putative back door region is located farther from the gorge entrance and closer to the N-terminal region, compared with the first molecule (Fig. 4, *A* and *B*). This second molecule is positioned within a second small depression, separated from the first one by ~9 Å and the protruding Asp^{131}. It interacts with residues that are mostly conserved, *e.g.* Leu^{22} in strand β0, Leu^{33} in β1, Phe^{65} in β3, Arg^{90} in the long Ω loop, and Asp^{131}, Asp^{134}, and Arg^{136} in the β3-α3,4 loop.

In both the SCh- and ATCh-S203A complexes, the surface-exposed side chain of Glu^{81} rotates, by 80°, to accommodate the bound ligand, but no significant conformational changes are detected elsewhere (Fig. 4, *D* and *E*). Should a shutter-like movement of the Trp^{86} side chain be involved in opening of a back door (28), our structures do not reveal it. Moreover, the presence of bound substrate in the back door region of the S203A mutant, but not mAChE, suggests limited affinity for this region compared with the base and entrance of the active center gorge. Next, in this region bound choline/TCh is absent in mAChE, despite identical soaking procedures. This suggests that this region does not provide an exit for the reaction products. Finally, an inhibitory antibody raised against *Electrophorus electricus* AChE was shown to bind to a surface site distinct from the PAS, and further identified as the region of the putative back door (63). In fact, the mAChE Asp^{460}-Gln^{474} segment that contains several SCh- and ATCh-interacting residues (Fig. 4), corresponds to the *E. electricus* AChE segment Glu^{484}-Arg^{498} shown, by mutagenesis analysis, to be involved in antibody binding (63). That binding of this antibody does not prevent inhibition by the substrate, as shown by the unaltered K_{ss} value, appears consistent with the absence of bound ACh in the back door region of the S203A mutant or bound substrate in this region on mAChE.

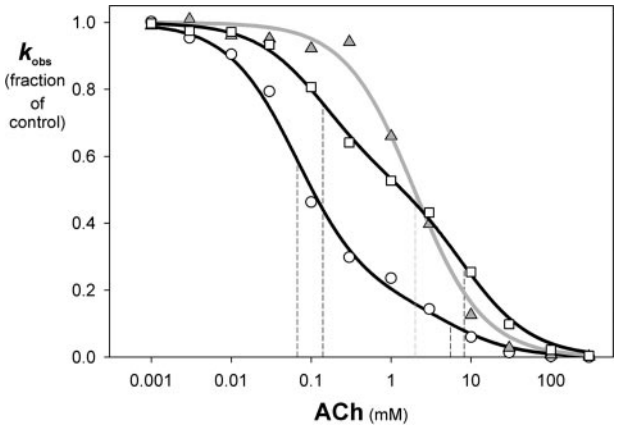

FIGURE 5. **Interaction of ACh with mAChE and S203A mutant.** The pseudo-first order association rates (k_{obs}) of ambenonium (5 μM; *circles*) and decidium (1 μM; *squares*) with mAChE, and of ambenonium (2 μM; *triangles*) with the S203A mutant in the presence of varying ACh concentrations are expressed as fractions of control rates measured in the absence of ACh (430 s^{-1} for ambenonium/mAChE, 320 s^{-1} for decidium/mAChE, and 103 s^{-1} for ambenonium/mutant). For each curve, experimental points corresponding to an average of two to four parallel rate measurements were fit to a biphasic (mAChE) or monophasic (mutant) binding isotherm. The ACh concentrations corresponding to inflection points are indicated (*dashed lines*).

Secondary binding sites for the PAS ligands propidium, decidium, and gallamine were not observed in structures of mAChE complexes (19) even though cocrystallization used ligand concentrations higher than those used for crystal soaking. This also argues for specific, although low affinity, binding of the substrates to the back door region.

Inhibition Kinetics and Binding of Substrates and Reversible Inhibitors

Inhibition, by SCh, 4K-TMA, and choline, of ATCh hydrolysis catalyzed by mAChE yielded constant (K_i) values close to the dissociation constant (K_d) values determined by competition (Table 2). The K_d values for interaction of SCh, BTCh, 4K-TMA, choline and of the rapidly hydrolyzed substrates ACh and ATCh with mAChE and the catalytically inactive S203A mutant, were determined from competition of the initial rate of binding of the reversible bisquaternary inhibitors, ambenonium (52) and decidium (53) (Fig. 5). These two compounds have the capacity to occupy both the active center gorge and the PAS, as shown for decamethonium or BW28C51 bound to crystalline TcAChE (34, 41), although decidium may preferably occupy the PAS, as seen in the crystalline mAChE complex (19).

Ambenonium and decidium competition yielded similar K_d values for most of the six ligands (Table 2). However, binding of

ACh or ATCh to mAChE caused a biphasic decrease of both the ambenonium and decidium association rates, yielding K_d and K_d^L values for each substrate (Fig. 5). The biphasic kinetics reflect formation of a ternary complex between the enzyme and associating and competing ligands. The K_d value, in the mid-micromolar range similar to the Michaelis constant (K_m) for ATCh, reflects interaction at the active center. The K_d^L value, in the millimolar range, approaches the substrate inhibition constant (K_{ss}, determined from the dependence of the rate of ATCh hydrolysis by mAChE on ATCh concentration) and reflects binding to the PAS. Association rates of both ambenonium and decidium thus decrease upon ACh or ATCh binding to and hydrolysis at the active center and further decrease upon their binding to the PAS. These K_d^L values, being slightly lower than the K_{ss} values for ACh and ATCh (Table 2), are consistent with constants derived from competition with fasciculin (11) and ambenonium (52).

A notable difference in the ambenonium and decidium competition data resides in the respective amplitudes of the two binding phases. The second phase, observed at higher ligand concentrations, is only one-fifth of the total amplitude in ambenonium competition but about half of the total amplitude in decidium competition (Fig. 5). The relative amplitudes reflect decidium association rates being less sensitive to ligand occupation at the active center than ambenonium rates, indicating that the decidium preference for the PAS more readily allows ternary complex formation. Yet, the limited specificity of decidium for PAS interactions, reflected by the similar ambenonium- and decidium-derived K_d values (Table 2), and its ability to detect binding of ACh or ATCh in the active center, reflected in the first inflection point, indicate binding of its charged trimethylammonio moiety deep within the gorge, in a position suitable for direct competition with the substrate. Hence, the decidium specificity for binding to the PAS resides mainly in its higher sensitivity to PAS competition. This is particularly evident in analysis of the 4K-TMA interaction with mAChE, where the second phase of binding is detected by decidium but not ambenonium.

The similarity in the K_d values for ACh, ATCh, and 4K-TMA binding to mAChE with the K_m for ATCh (Table 2) is consistent with formation of a covalent bond with Ser^{203} during the competition assay, as is evident during ACh and ATCh hydrolysis and demonstrated here for 4K-TMA binding to mAChE (Fig. 2*B*). The millisecond time interval of the competition assay for substrate interaction with mAChE allows for a few catalytic cycles of ACh (or ATCh) hydrolysis to elapse including covalent bond making and breaking.

The K_d values determined for the S203A mutant, where covalent bonding is not possible, are systematically greater than those for mAChE (Table 2). For the large substrates SCh and BTCh and for choline, the difference is only 2–3-fold, whereas for the small substrates ACh and ATCh and for 4K-TMA it is 10–20-fold. The catalytic cycles for SCh and BTCh hydrolysis by mAChE are more than 2 orders of magnitude slower than the duration of the competition assay. Hence the K_d values determined for these two substrates represent their true dissociation constants. For ACh, ATCh, and 4K-TMA, the higher K_d values, being greater than the K_m for ATCh and mAChE, likely reflect unfavorable binding orientations in the mutant, as observed in the ACh- and ATCh-S203A complexes (Fig. 2, *C* and *D*), and consistent with the absence of bound 4K-TMA in the crystalline mutant (see above). This suggests that the structures of the ACh- and ATCh-S203A complexes may differ from the reversible Michaelis complex of ACh with mAChE.

The low millimolar K_d values observed for the 4K-TMA, ACh, and ATCh interaction with mAChE likely reflect binding to the PAS as seen in the structures (Fig. 2, *B–D*). In contrast, the PAS interactions of SCh and BTCh observed in the structures (Fig. 2, *E–G*) were not resolved in the competition binding assays. In the S203A mutant, the loss of affinity at the active site may preclude detection of active site and PAS interactions.

Implications for AChE Catalysis and Regulation

This set of eight structures, in highlighting distinctive positions, orientations, and conformations of various substrates and analogues and a product trapped in the crystalline wild type or mutant mAChE, along with the binding and inhibition data obtained on the same complexes, led us to suggest a succession of steps that may contribute to understanding catalysis and its regulation by high substrate concentrations. Complexes with an analogue and a substrate anchored to Glu^{202} and His^{447} within the active site pocket and oriented perpendicular to the gorge axis (TMTFA-, 4K-TMA-, and SCh-mAChE conjugates; Fig. 2, *A*, *B*, and *F*) clearly reflect acylation transition states and an acyl-enzyme. They also illustrate the key role of the aromatic Trp^{86} and charged Glu^{202} side chains in selective orientation of the ligand within the active site, through cation-π interaction and longer range (4.2–4.5 Å) electrostatic interactions, respectively. Complexes of the S203A mutant with intact ACh and ATCh molecules that are rotated compared with the hemiketal conformation and still bound, via their quaternary ammonium group, to the anionic subsite of the active center (Fig. 2, *C* and *D*), likely reflect the deacetylated enzyme structure**.** In turn, the choline or TCh molecule bound in the active site (Fig. 2, *D*, *G*, and *H*) and those bound to the PAS and aligned with the gorge dipole moment (Fig. 2, *D* and *H*), must mimic the dissociating and the egressing products, respectively.

Because of the high soaking concentrations necessary to observe PAS-bound ligands in the structures, the substrates or substrate analogues anchored, via their quaternary ammonium group, to Trp^{286} in the PAS and aligned against the gorge dipole moment (*cf.* Fig. 2, *B*, *C*, and *E–G*), likely reflect binding associated with substrate inhibition. Hence, substrate in excess will slow down the exit of the choline product both by electrostatic repulsion, via its acetyl group, and by steric occlusion of the gorge entrance. In fact, these substrates or analogues may also reflect the incoming substrate, initially attracted via its acetyl group by the PAS, and now transiently occupying the gorge entrance before it proceeds toward the active center. Hence, the PAS-bound substrate would simply slide down into the gorge, to place the acyl carbon in a position suitable for attack by the Ser hydroxyl, and then reorient to stabilize the quaternary ammonium group within the anionic subsite. This motion would be associated with rearrangement of the substrate from the non-relaxed *trans*, *trans* conformation adopted at the

PAS to the presumably more labile relaxed *trans*, *gauche* conformation adopted in the active center, along with major although transient rearrangements of side chains within the gorge, such as those of Tyr^{337} and Tyr^{124} as observed in the structures. Finally, substrate binding in the putative back door region (Fig. 4), although lacking a structurally or functionally evident portal of entry, could allosterically affect substrate binding and catalytic parameters.

In conclusion, in the crystalline mAChE and S203A mutant we identified several successive positions and orientations of the substrates bound to the PAS at the gorge entrance and proceeding within the gorge toward the active site; the conformation of the acylation transition state and acyl-enzyme; the positions and orientations of the dissociating and egressing products; and those of intact substrate molecules stably bound at secondary sites in the region of the putative back door. The lability of the substrate and intermediates in the pathway requires that surrogate structures be used in several cases. Nevertheless, these structures provide a comprehensive set of snapshots of the routes for traffic of substrates and products, the reaction intermediates along the gorge pathway, and perhaps, allosteric regulation of catalysis by substrate binding to low affinity sites at the enzyme surface.

After a revised version of this manuscript was submitted, an article was published on-line (65) that reported structural data with some common substrates and analogues and yielded similar conclusions despite differences in experimental conditions. Our study considers additional ligands, provides a kinetic analysis of ligand association, and identifies new binding sites on the enzyme surface.

Acknowledgments—Expert assistance from the European Synchrotron Radiation Facility staff is much appreciated. We thank Harvey A. Berman (State University of New York at Buffalo) and Daniel M. Quinn (University of Iowa) for the gifts of decidium and TMTFA, respectively; Sventja von Daake (University of California, San Diego) for purification of mAChE; and Marianick Juin (CNRS FRE-2738) and Jordan Ménard (CNRS UMR-6098) for assistance in crystallogenesis and structure resolution, respectively.

REFERENCES

1. Massoulie, J., Sussman, J., Bon, S., and Silman, I. (1993) *Prog. Brain Res.* **98,** 139–146
2. Taylor, P., and Radić, Z. (1994) *Annu. Rev. Pharmacol. Toxicol.* **34,** 281–320
3. Rachinsky, T. L., Camp, S., Li, Y., Ekstrom, T. J., Newton, M., and Taylor, P. (1990) *Neuron* **5,** 317–327
4. Sussman, J. L., Harel, M., Frolow, F., Oefner, C., Goldman, A., Toker, L., and Silman, I. (1991) *Science* **253,** 872–879
5. Bourne, Y., Taylor, P., and Marchot, P. (1995) *Cell* **83,** 503–512
6. Froede, H. C., and Wilson, I. B. (1984) *J. Biol. Chem.* **259,** 11010–11013
7. Changeux, J. P. (1966) *Mol. Pharmacol.* **2,** 369–392
8. Taylor, P., and Lappi, S. (1975) *Biochemistry* **14,** 1989–1997
9. Mooser, G., and Sigman, D. S. (1974) *Biochemistry* **13,** 2299–2307
10. Radić, Z., Reiner, E., and Taylor, P. (1991) *Mol. Pharmacol.* **39,** 98–104
11. Szegletes, T., Mallender, W. D., Thomas, P. J., and Rosenberry, T. L. (1999) *Biochemistry* **38,** 122–133
12. Mallender, W. D., Szegletes, T., and Rosenberry, T. L. (2000) *Biochemistry* **39,** 7753–7763
13. Johnson, J. L., Cusack, B., Hughes, T. F., McCullough, E. H., Fauq, A., Romanovskis, P., Spatola, A. F., and Rosenberry, T. L. (2003) *J. Biol. Chem.* **278,** 38948–38955
14. Johnson, J. L., Cusack, B., Davies, M. P., Fauq, A., and Rosenberry, T. L. (2003) *Biochemistry* **42,** 5438–5452
15. Radić, Z., Pickering, N. A., Vellom, D. C., Camp, S., and Taylor, P. (1993) *Biochemistry* **32,** 12074–12084
16. Shafferman, A., Kronman, C., Flashner, Y., Leitner, M., Grosfeld, H., Ordentlich, A., Gozes, Y., Cohen, S., Ariel, N., and Barak, D. (1992) *J. Biol. Chem.* **267,** 17640–17648
17. Barak, D., Kronman, C., Ordentlich, A., Ariel, N., Bromberg, A., Marcus, D., Lazar, A., Velan, B., and Shafferman, A. (1994) *J. Biol. Chem.* **269,** 6296–6305
18. Harel, M., Kleywegt, G. J., Ravelli, R. B., Silman, I., and Sussman, J. L. (1995) *Structure* **3,** 1355–1366
19. Bourne, Y., Taylor, P., Radić, Z., and Marchot, P. (2003) *EMBO J.* **22,** 1–12
20. Bourne, Y., Kolb, H. C., Radić, Z., Sharpless, K. B., Taylor, P., and Marchot, P. (2004) *Proc. Natl. Acad. Sci. U. S. A.* **101,** 1449–1454
21. Nachmansohn, D., and Wilson, I. B. (1951) *Adv. Enzymol. Relat. Subj. Biochem.* **12,** 259–339
22. Aldridge, W. N., and Reiner, E. (1969) *Biochem. J.* **115,** 147–162
23. Marcel, V., Palacios, L. G., Pertuy, C., Masson, P., and Fournier, D. (1998) *Biochem. J.* **329,** 329–334
24. Stojan, J., Marcel, V., Estrada-Mondaca, S., Klaebe, A., Masson, P., and Fournier, D. (1998) *FEBS Lett.* **440,** 85–88
25. Karlsson, E., Mbugua, P. M., and Rodriguez-Ithurralde, D. (1984) *J. Physiol.* **79,** 232–240
26. Marchot, P., Khelif, A., Ji, Y. H., Mansuelle, P., and Bougis, P. E. (1993) *J. Biol. Chem.* **268,** 12458–12467
27. Axelsen, P. H., Harel, M., Silman, I., and Sussman, J. L. (1994) *Protein Sci.* **3,** 188–197
28. Gilson, M. K., Straatsma, T. P., McCammon, J. A., Ripoll, D. R., Faerman, C. H., Axelsen, P. H., Silman, I., and Sussman, J. L. (1994) *Science* **263,** 1276–1278
29. Eastman, J., Wilson, E. J., Cervenansky, C., and Rosenberry, T. L. (1995) *J. Biol. Chem.* **270,** 19694–19701
30. Radić, Z., Duran, R., Vellom, D. C., Li, Y., Cervenansky, C., and Taylor, P. (1994) *J. Biol. Chem.* **269,** 11233–11239
31. Radić, Z., Quinn, D. M., Vellom, D. C., Camp, S., and Taylor, P. (1995) *J. Biol. Chem.* **270,** 20391–20399
32. Bartolucci, C., Perola, E., Cellai, L., Brufani, M., and Lamba, D. (1999) *Biochemistry* **38,** 5714–5719
33. Bencharit, S., Morton, C. L., Howard-Williams, E. L., Danks, M. K., Potter, P. M., and Redinbo, M. R. (2002) *Nat. Struct. Biol.* **9,** 337–342
34. Harel, M., Schalk, I., Ehret-Sabatier, L., Bouet, F., Goeldner, M., Hirth, C., Axelsen, P. H., Silman, I., and Sussman, J. L. (1993) *Proc. Natl. Acad. Sci. U. S. A.* **90,** 9031–9035
35. Raves, M. L., Harel, M., Pang, Y. P., Silman, I., Kozikowski, A. P., and Sussman, J. L. (1997) *Nat. Struct. Biol.* **4,** 57–63
36. Ravelli, R. B., Raves, M. L., Ren, Z., Bourgeois, D., Roth, M., Kroon, J., Silman, I., and Sussman, J. L. (1998) *Acta Crystallogr. Sect. D Biol. Crystallogr.* **54,** 1359–1366
37. Bartolucci, C., Perola, E., Pilger, C., Fels, G., and Lamba, D. (2001) *Proteins* **42,** 182–191
38. Bar-On, P., Millard, C. B., Harel, M., Dvir, H., Enz, A., Sussman, J. L., and Silman, I. (2002) *Biochemistry* **41,** 3555–3564
39. Millard, C. B., Kryger, G., Ordentlich, A., Greenblatt, H. M., Harel, M., Raves, M. L., Segall, Y., Barak, D., Shafferman, A., Silman, I., and Sussman, J. L. (1999) *Biochemistry* **38,** 7032–7039
40. Kryger, G., Silman, I., and Sussman, J. L. (1998) *J. Physiol.* **92,** 191–194
41. Felder, C. E., Harel, M., Silman, I., and Sussman, J. L. (2002) *Acta Crystallogr. Sect. D Biol. Crystallogr.* **58,** 1765–1771
42. Harel, M., Quinn, D. M., Nair, H. K., Silman, I., and Sussman, J. L. (1996) *J. Am. Chem. Soc* **118,** 2340–2346
43. Marchot, P., Ravelli, R. B., Raves, M. L., Bourne, Y., Vellom, D. C., Kanter, J., Camp, S., Sussman, J. L., and Taylor, P. (1996) *Protein Sci.* **5,** 672–679
44. Otwinowski, Z., and Minor, W. (1997) *Methods Enzymol.* **276,** 307–326
45. CCP4 (1994) *Acta Crystallogr. Sect. D Biol. Crystallogr.* **50,** 760–763
46. Murshudov, G. N., Vagin, A. A., and Dodson, E. J. (1997) *Acta Crystallogr.*

Sect. D Biol. Crystallogr. **53,** 240–255
47. Perrakis, A., Morris, R., and Lamzin, V. S. (1999) *Nat. Struct. Biol.* **6,** 458–463
48. Emsley, P., and Cowtan, K. (2004) *Acta Crystallogr. Sect. D Biol. Crystallogr.* **60,** 2126–2132
49. Laskowski, R., MacArthur, M., Moss, D., and Thornton, J. (1993) *J. Appl. Crystallogr.* **26,** 283–291
50. DeLano, W. L. (2002) *The PyMOL Molecular Graphics System*, DeLano Scientific, San Carlos, CA
51. Ellman, G. L., Courtney, K. D., Andres, V., Jr., and Feather-Stone, R. M. (1961) *Biochem. Pharmacol.* **7,** 88–95
52. Hodge, A. S., Humphrey, D. R., and Rosenberry, T. L. (1992) *Mol. Pharmacol.* **41,** 937–942
53. Berman, H. A., and Decker, M. M. (1986) *Biochim. Biophys. Acta* **872,** 125–133
54. Radić, Z., and Taylor, P. (2001) *J. Biol. Chem.* **276,** 4622–4633
55. Kryger, G., Silman, I., and Sussman, J. L. (1999) *Struct. Fold Des.* **7,** 297–307
56. Canepa, F. G., Pauling, P., and Sorum, H. (1966) *Nature* **210,** 907–909
57. Partington, P., Feeney, J., and Burgen, A. S. (1972) *Mol. Pharmacol.* **8,** 269–277
58. Nicolet, Y., Lockridge, O., Masson, P., Fontecilla-Camps, J. C., and Nachon, F. (2003) *J. Biol. Chem.* **278,** 41141–41147
59. Shi, J., Boyd, A. E., Radić, Z., and Taylor, P. (2001) *J. Biol. Chem.* **276,** 42196–42204
60. Shi, J., Tai, K., McCammon, J. A., Taylor, P., and Johnson, D. A. (2003) *J. Biol. Chem.* **278,** 30905–30911
61. Boyd, A. E., Dunlop, C. S., Wong, L., Radić, Z., Taylor, P., and Johnson, D. A. (2004) *J. Biol. Chem.* **279,** 26612–26618
62. Bui, J. M., and McCammon, J. A. (2005) *Chem. Biol. Interact.* **157–158**, 357–359
63. Simon, S., Le Goff, A., Frobert, Y., Grassi, J., and Massoulie, J. (1999) *J. Biol. Chem.* **274,** 27740–27746
64. Hosea, N. A., Berman, H. A., and Taylor, P. (1995) *Biochemistry* **34,** 11528–11536
65. Colletier, J. P., Fournier, D., Greenblatt, H. M., Stojan, J., Sussman, J. L., Zaccai, G., Silman, I., and Weik, M. (2006) *EMBO J.* **25,** 2746–2756
66. Roussel, A., and Cambillau, C. (1989) *TURBO-FRODO; Silicon Graphics Geometry Partners Directory* (Silicon Graphics Committee, ed) Mountain View, CA